Magnetic structure of Nd in NdFeAsO studied by x-ray resonant magnetic scattering

M. G. Kim,[1,2,*] J.-W. Kim,[3] J.-Q. Yan,[2,†] A. I. Goldman,[2] and A. Kreyssig[2]

[1]*Department of Physics and Astronomy, Rutgers University, Piscataway, New Jersey 08854, USA*

[2]*Ames Laboratory, U.S. DOE and Department of Physics and Astronomy, Iowa State University, Ames, Iowa 50011, USA*

[3]*Advanced Photon Source, Argonne National Laboratory, Argonne, Illinois 60439, USA*

(Received 11 July 2019; revised manuscript received 11 October 2019; published 2 December 2019)

The magnetic structure of Nd in NdFeAsO compound has been investigated by x-ray resonant magnetic scattering at the Nd L_2 edge ($E = 6.725$ keV) at $1.7 \leqslant T \leqslant 15$ K. At $T = 1.7$ K we find that the Nd moments are aligned along the crystallographic c direction with the (1, 0, 0) propagation vector, and are arranged antiferromagnetically along the a direction and ferromagnetically along the b and c directions. At $1.7 < T \leqslant 15$ K, we observe an unusual temperature dependence of the magnetic Bragg peaks that appear differently at $\mathbf{Q} = (h, 0, l)$ and $(0, k, l)$. From the changes of magnetic intensities and our representation analysis, we find that the Nd moments are reoriented toward the a direction with a gradual decrease of the moment component in the c direction with increasing temperature. We conclude that the reorientation of the Nd moment is due to a strong interplay with the Fe moment which is fully ordered in this temperature range.

DOI: 10.1103/PhysRevB.100.224401

I. INTRODUCTION

Since the discovery of superconductivity (SC) in $LaFeAsO_{1-x}F_x$ [1], the magnetism and its role for the SC have been studied extensively [2–4]. Having the Fe magnetism as an essential ingredient for the unconventional SC in the Fe-based superconductors (pnictides) was surprising based on the conventional antagonism of magnetism and superconductivity. More interestingly, among many pnictides, higher superconducting transition temperatures (T_c) were found in compounds with additional magnetic elements, the oxypnictide superconductors $RE\text{FeAsO}_{1-x}\text{F}_x$ (RE = rare-earth elements) [2]. One reason for the enhanced T_c in the oxypnictides can be due to the variation of geometric factors [2,5]. It is also possible that a strong interplay between magnetism from $4f$ electrons and $3d$ electrons [6–17] enhances magnetic fluctuations that mediate the superconducting pairing mechanism [2–4].

To understand the interplay between two different magnetic species, the magnetic structures of several rare-earth oxypnictides were studied by neutron diffraction, μSR, Mössbauer, and x-ray resonant magnetic scattering measurements [6–17]. Many of the magnetic structures of REFeAsO (RE = Ce, Pr, Nd, and Sm) were identified, but some reported magnetic structures are still in debate. For instance, while the magnetic structures of Ce and Sm are known and consistently confirmed by other reports [6,12,14,16], for Pr and Nd different antiferromagnetic (AFM) structures were suggested in some studies [7,8,10–12,15,17]. In the family of PrFeAsO compounds, at low temperature, neutron powder diffraction (NPD) measurements found an AFM structure in which the Pr moments align antiferromagnetically in the ab plane and ferromagnetically along the c axis with the moment pointing along the c axis [7,8], but a μSR study claimed the same magnetic arrangements as in NPD except the Pr moments pointing along the a axis [12].

In the NdFeAsO compound, the tetragonal-to-orthorhombic structural transition occurs below $T_S \approx 150$ K and Fe orders antiferromagnetically below $T_{Fe} \approx 140$ K followed by the magnetic ordering of Nd below $T_{Nd} \approx 5$ K [9–11,15]. Due to an interconnection between Fe and Nd, induced Nd moments or coupled Fe and Nd moments appear at $T = T^* \approx 15$ K [15]. A NPD measurement claimed that the Nd moments lie in the $\boldsymbol{ac}$ plane with similar sizes of moment components in the a and c directions. It showed an AFM structure with antiferromagnetic arrangement in the ab plane and ferromagnetic alignment along the c axis [10]. Single crystal neutron diffraction measurements found that the measured magnetic Bragg peaks are consistent with the proposed magnetic structure [15]. Later, another NPD measurement proposed a different magnetic structure with Nd moments pointing along the a axis [17]. Because Nd moments are coupled with Fe moments at $T^* \approx 15$ K [15] and neutron measurements probe overall magnetic signals from Fe and Nd indiscernibly, it is difficult to identify the precise magnetic structure and understand the complex interplay between Nd and Fe. Model calculations for the magnetic anisotropy yield the result that the easy axis for the Nd moments should be the b axis [18].

Here we report the low-temperature magnetic structure of Nd and a temperature-dependent reorientation of Nd moment in the parent NdFeAsO compound. We employed the element-specific x-ray resonant magnetic scattering (XRMS) technique that probes Nd magnetism separately from Fe magnetism by tuning the incoming x-ray energy to the Nd L_2 absorption edge. From the measured magnetic Bragg peak intensities and the symmetry analysis, we find that, at low

*mgkim@physics.rutgers.edu

†Present address: Materials Science and Technology Division, Oak Ridge National Laboratory, Oak Ridge, Tennessee 37831, USA.

temperature, the Nd moments point along the c axis with antiferromagnetic alignment in the a direction and ferromagnetic arrangement along the b and c axes. Detailed temperature-dependent measurements of the magnetic Bragg peaks indicate that the Nd moments are reoriented toward the a direction (which was absent at low temperature) with a gradual decrease of the moment component in the c direction with increasing temperature.

II. EXPERIMENT

Single crystals of NdFeAsO were grown out of a NaAs flux using the conventional high-temperature solution growth technique as described in Ref. [19]. The stoichiometry of samples from a growth batch was examined by wavelength dispersive spectroscopy in a JEOL JXA-8200 Superprobe electron probe microanalyzer. Specific heat and resistivity were measured on multiple samples from the same growth batch which showed excellent homogeneity of the samples [15]. Crystals from the same batch were studied by both neutron and x-ray diffraction measurements previously [15]. For the XRMS measurements, an as-grown platelike single crystal with dimensions of approximately $2 \times 2 \times 0.08$ mm^3 was selected. The surface of the crystal was perpendicular to the c axis. The XRMS experiment was conducted on the beamline 6-ID-B at the Advanced Photon Source at Argonne National Laboratory at the Nd L_2 edge ($E = 6.725$ keV). The incident radiation was linearly polarized perpendicular to the vertical scattering plane (σ polarized) with a spatial cross section of 0.5 mm (horizontal) $\times$ 0.2 mm (vertical). In this configuration, dipole resonant magnetic scattering rotates the scattered beam polarization into the scattering plane (π polarization). Cu(2, 2, 0) was used as a polarization and energy analyzer to suppress the charge and fluorescence background relative to the magnetic scattering signal. The sample was mounted at the end of the cold finger of a closed cycle He Joule-Thomson cryostat ($1.7 \leqslant T \leqslant 18$ K) with the orthorhombic $(H, 0, L)$ or $(0, K, L)$ planes coincident with the scattering plane.

III. RESULTS

We first examine magnetic reflections at the Nd L_2 edge. Figure 1(a) displays the resonant behavior measured at $T =$ 3 K and at the (1, 0, 5) magnetic Bragg peak position together with the fluorescence signal obtained under the same experimental conditions. We observed an enhanced intensity in the σ-π scattering channel approximately 3 eV above the absorption edge, indicating that the observed intensity is the dipole resonance. Similar dipole resonant peaks and their energy dependence were previously reported at L edges in rare-earth elements [20,21].

At $T = 3$ K ($T < T_{\mathrm{Nd}}$), the orthorhombic structure may have four twin domains that appear as four Bragg peaks at slightly different **Q** positions [22]. **Q** scans were performed along high symmetry directions to identify orthorhombic twin domains in the sample. Figure 1(b) shows two structural Bragg peaks observed in **Q** scans along [0, K, 0]. The (2, 0, 6) peak is originated from a domain with the longer orthorhombic a axis in the scattering plane, and the (0, 2, 6) peak is from a domain with the shorter orthorhombic b axis in the scattering plane. From different **Q** scans we can identify all peaks from four twin domains in the reciprocal space as shown in Fig. 1(d). Then we searched for magnetic reflections with respect to the observed orthorhombic twin domains. We again find four magnetic Bragg reflections at positions corresponding to four different orthorhombic twin domains around $\mathbf{Q} = (1, 0, 6)$ and (0, 1, 6) [Figs. 1(c) and 1(e)]. Magnetic Bragg peaks were also observed at $\mathbf{Q} = (1, 0, 5)$ and (0, 1, 5) in Fig. 3, consistent with a propagation vector (1, 0, 0). The XRMS in the σ-π scattering channel is only sensitive to spin components lying in the scattering plane. For instance, Fe moments in the pnictides pointing along the orthorhombic a axis would produce the magnetic Bragg peaks only at **Q** positions characterized by the longer orthorhombic a axis [16,23], e.g., at (1, 0, 6) and (1, 0, 6)′, but no magnetic Bragg peak at, e.g., (0, 1, 6) and (0, 1, 6)′ (see Table I). Observation of Nd magnetic peaks from all orthorhombic twin domains indicates that Nd moments do not simply point along the orthorhombic a (or b) axis, which would give peaks at **Q** positions only from domains characterized by the longer a (or the shorter b) axis.

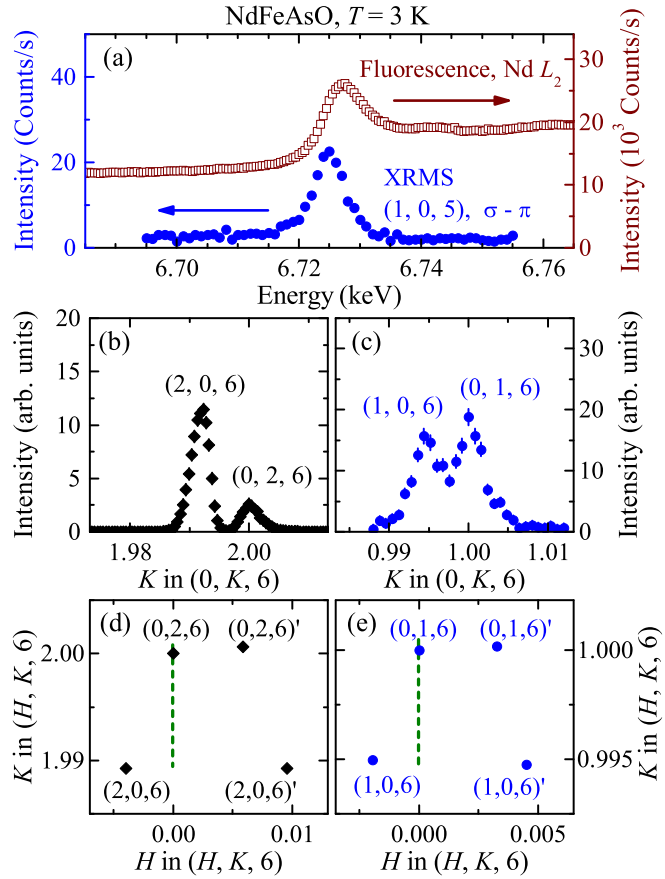

FIG. 1. (a) Energy scans through the (1, 0, 5) magnetic Bragg peak (filled circles) in the σ-π scattering geometry at $T = 3$ K and the measured fluorescence (open squares) under the same experimental conditions without a polarization analyzer. (b) [0, K, 0] scan through the structural Bragg position at $T = 3$ K. (c) [0, K, 0] scan through the magnetic Bragg position at $T = 3$ K. (d) and (e) Plot of the structural and magnetic peak positions in the H and K planes, respectively. The dashed lines indicate the scan path in (b) and (c).

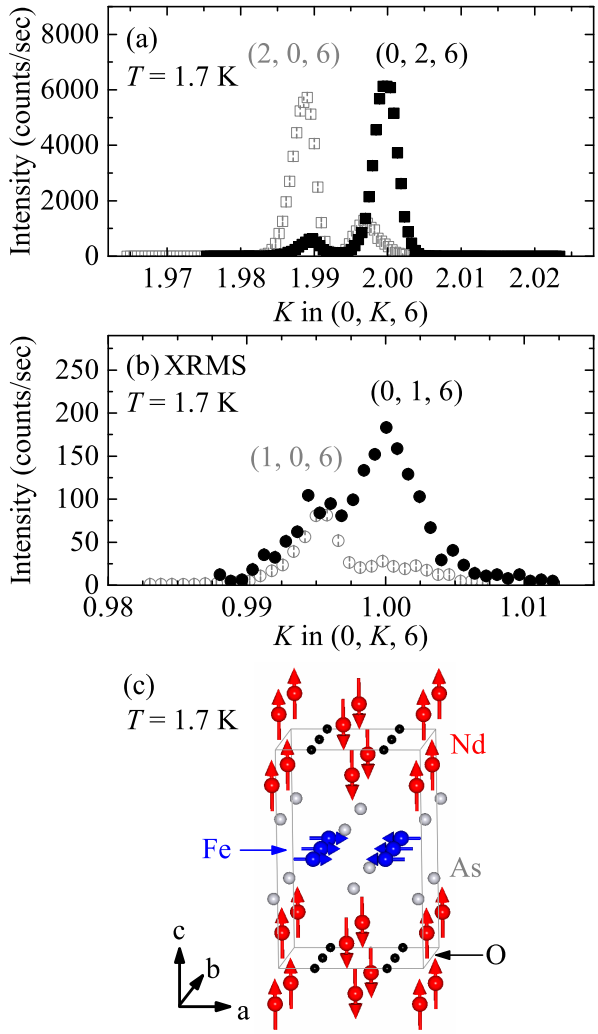

FIG. 2. Distribution of (a) structural Bragg peaks measured along [0, K, 0] after the alignment is optimized for $\mathbf{Q} = (2, 0, 6)$ (open squares) and for (0, 2, 6) (filled squares), respectively and (b) magnetic Bragg peaks measured along [0, K, 0] after the alignment is optimized for $\mathbf{Q} = (1, 0, 6)$ (open circles) and for (0, 1, 6) (filled circles), respectively. (c) Proposed magnetic structure at $T = 1.7$ K.

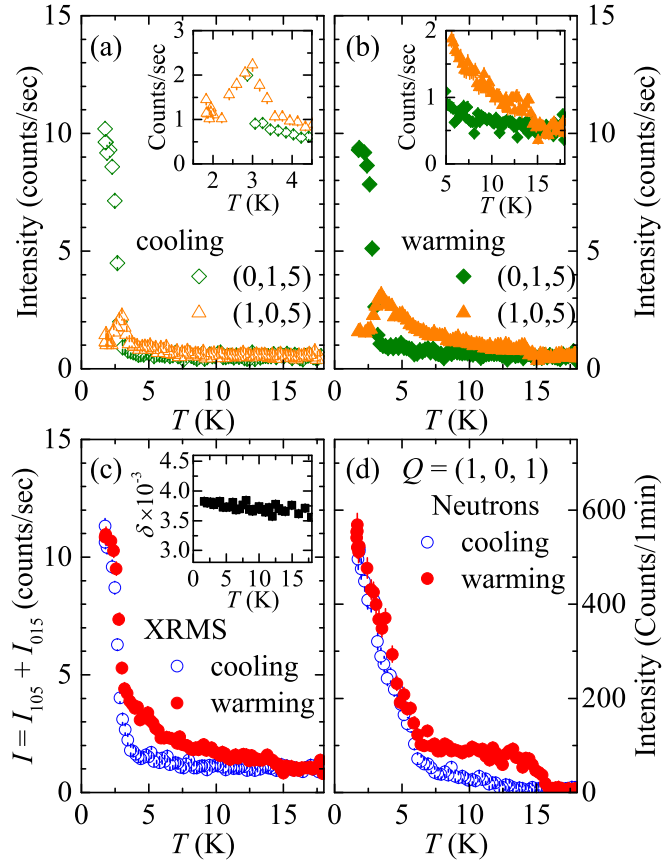

FIG. 3. Temperature dependence of the magnetic order parameters of the magnetic (1, 0, 5) (triangles) and (0, 1, 5) (diamonds) Bragg peaks during (a) cooling (open symbols) and (b) warming (filled symbols). Insets in (a) and (b) show the temperature range between 1.7 and 5 K and between 5 and 18 K, respectively. (c) Total scattering intensity by sum of intensities of (1, 0, 5) and (0, 1, 5) Bragg peaks during cooling (open circles) and warming (filled circles). Inset shows the orthorhombicity $\delta = (a - b)/(a + b)$ in the same temperature range. (d) The magnetic order parameter at $\mathbf{Q} = (1, 0, 1)$ from our previous neutron diffraction measurement [15] during cooling (open circles) and warming (filled circles).

We can exclude the magnetic structure proposed by Ref. [17], where moments point along the orthorhombic a axis.

To determine the magnetic moment configuration for the Nd moments, we performed representation analysis [24] for the *Cmme* space group and the (1, 0, 0) propagation vector for the Nd order [10,11,15]. Table I shows six independent magnetic representations (MRs) and the allowed reflections for the scattering geometry used in our experiment. There are four crystallographically equivalent Nd atoms: atom 1 at (0, 0.25, 0.1389), atom 2 at (0, 0.75, 0.8611), atom 3 at (0.5, 0.75, 0.1389), and atom 4 at (0.5, 0.25, 0.8611). In all MRs, Nd moments at the C-centered atoms 1 and 3 are arranged antiferromagnetically, similarly at atoms 2 and 4. The MRs Γ_6 and Γ_7 allow Nd magnetic moment along the a axis, Γ_8 and Γ_5 along the b axis, and Γ_2 and Γ_3 along the c axis. Of the two MRs for a particular Nd moment direction, the first one represents antiferromagnetic alignment of the Nd magnetic moments between atom 1 and atom 2 (atoms 3 and 4) and the second one represents ferromagnetic alignment of the Nd magnetic moments between atom 1 and atom 2 (atoms 3 and 4). As we discussed earlier, the MRs Γ_5, Γ_6, Γ_7, and Γ_8 can be excluded because these MRs only produce magnetic Bragg peaks either at $\mathbf{Q} = (h, 0, l)$ or $(0, k, l)$. Then the possible MRs for Nd magnetic moment configuration are Γ_2 and Γ_3 that allow moments along the c direction. To distinguish the difference between Γ_2 and Γ_3 MRs, we calculated the XRMS intensities for each MR. The XRMS intensity is proportional to the magnetic structure factor $|F_m|^2$,

$$I \propto |F_m|^2. \tag{1}$$

The magnetic structure amplitude for (h, k, l) is

$$F_m = \sum_j f_j e^{2\pi i(hx_j + ky_j + lz_j)}. \tag{2}$$

f_j is the resonant magnetic scattering amplitude [25]

$$f_j = f_{\mathrm{XRMS}} = -iC\mu[z_3 \sin(\theta + \alpha) - z_1 \cos(\theta + \alpha)], \tag{3}$$

TABLE I. Magnetic representations (MRs) for NdFeAsO for the space group *Cmme* with a propagation vector (1, 0, 0). The decomposition of the MR for the Nd site (0, 0.25, 0.1389) is $\Gamma_{mag} = \Gamma_2 + \Gamma_3 + \Gamma_5 + \Gamma_6 + \Gamma_7 + \Gamma_8$. The atoms of the primitive basis are defined according to 1 (0, 0.25, 0.1389), 2 (0, 0.75, 0.8611). Lattice parameters of the orthorhombic structure at 0.3 K: $a = 5.6159$ Å, $b = 5.587$ Å, $c = 8.557$ Å [10].

					Magnetic intensity	
		BV components			$(h, 0, l)$	$(0, k, l)$
IR	Atom	$m \parallel a$	$m \parallel b$	$m \parallel c$	$\sigma \rightarrow \pi$	$\sigma \rightarrow \pi$
Γ_2	1	0	0	1	Yes	Yes
	2	0	0	−1		
Γ_3	1	0	0	1	Yes	Yes
	2	0	0	1		
Γ_5	1	0	1	0	No	Yes
	2	0	1	0		
Γ_6	1	1	0	0	Yes	No
	2	−1	0	0		
Γ_7	1	1	0	0	Yes	No
	2	1	0	0		
Γ_8	1	0	1	0	No	Yes
	2	0	−1	0		

where C is a scaling constant, μ is the magnetic moment, 2θ is the scattering angle, α is the angle between the scattering vector $\mathbf{Q}$ and the c axis perpendicular to the sample surface, and z_1 and z_3 are the two orthogonal spin components in the scattering plane. Using the equations, the magnetic peak intensities were calculated at $\mathbf{Q} = (1, 0, 6)$, $(0, 1, 6)$, $(1, 0, 5)$, and $(0, 1, 5)$ for Γ_2 and Γ_3 MRs. We find the intensity ratios $I_{106}/I_{016} = 2.9$ and 0.34 and $I_{105}/I_{015} = 7.7$ and 0.13 for Γ_2 and Γ_3, respectively. To compare these values with experimental values, the domain population of orthorhombic twin domains were carefully characterized at $T = 1.7$ K because less populated domains can produce reduced magnetic intensities even if the ordered magnetic moments are the same in all domains. Several angle scans (alignment scans) were performed through structural Bragg peaks from all domains to maximize their intensities. Before the alignment [Fig. 1(b)], highly unbalanced diffraction intensities were observed for each domain, but after the alignment, we find that (2, 0, 6) and (0, 2, 6) domains are almost equally populated as shown in Fig. 2(a). The ratio between (2, 0, 6) and (0, 2, 6) domains is 1:1.1. The measured magnetic Bragg peak intensities at positions corresponding to two twin domains are shown for the (1, 0, 6) and (0, 1, 6) magnetic Bragg peaks in Fig. 2(b) and for the (1, 0, 5) and (0, 1, 5) magnetic Bragg peaks in Fig. 3. We find the measured intensity ratios $I_{106}/I_{016} = 0.36 \pm 0.03$ and $I_{105}/I_{015} = 0.15 \pm 0.04$. These values are surprisingly close to the calculated values (0.34 and 0.13, respectively) for Γ_3 MR. The Γ_3 magnetic structure of Nd at $T = 1.7$ K is shown in Fig. 2(c) together with the Fe moment configuration from Refs. [9,10]. Our magnetic structure of Nd is different from the magnetic structures proposed in Ref. [17], but somewhat similar to the magnetic structure proposed in Ref. [10], which has moment components in the c as well as in the a direction. The slightly higher intensity ratio from our measurement might be due to a small Nd moment component in the a direction which will produce additional intensity at $\mathbf{Q} = (h, 0, l)$. However, our observation indicates that the moment component in the a direction would be much smaller than the moment component in the c direction which is different from the magnetic structure in Ref. [10] that reported comparable moment sizes in the a and c directions. Interestingly, Pr and Sm moments also align in the c direction in PrFeAsO [7,8] and SmFeAsO compounds [14,16] in the same antiferromagnetic alignment as have been concluded for NdFeAsO at low temperatures here. Magnetism in these compounds may share similar underlying physics.

We now turn to the temperature dependence of Nd magnetic ordering. The magnetic Bragg peak intensities at $\mathbf{Q} = (1, 0, 5)$ and (0, 1, 5) were measured during cooling and warming between 1.7 and 18 K and show an unusual temperature dependence. During cooling [Fig. 3(a)], while the intensity at $\mathbf{Q} = (1, 0, 5)$ gradually appears below $T \approx 10$ K, the intensity at $\mathbf{Q} = (0, 1, 5)$ starts to appear only below $T \approx 5$ K. Between $T \approx 3$ and 5 K we observed slightly more intensity at $\mathbf{Q} = (1, 0, 5)$ than at $\mathbf{Q} = (0, 1, 5)$ [the inset in Fig. 3(a)]. The (1, 0, 5) magnetic peak reaches its maximum intensity at $T \approx 3$ K and weakens gradually, whereas the (0, 1, 5) peak rapidly grows below $T < 3$ K. Figure 3(b) shows the magnetic order parameters during warming. The magnetic peak intensity at $\mathbf{Q} = (0, 1, 5)$ decreases fast with increasing temperature which is consistent with the behavior observed during cooling. The (0, 1, 5) peak intensity almost disappears at $T_{Nd} = 3$ K which is consistent with Ref. [10] but slightly lower than T_{Nd} in Ref. [15], which is likely due to x-ray beam heating effects. The magnetic intensity measured at $\mathbf{Q} = (1, 0, 5)$, however, shows a hysteretic behavior. We observed higher intensity at $\mathbf{Q} = (1, 0, 5)$ in temperatures between $1.7 < T < 15$ K $(= T^*)$ during warming than during cooling. Such a behavior is emphasized in the inset of Fig. 3(b). While we find that the (0, 1, 5) magnetic peak decreases gradually with increasing the temperature, the (1, 0, 5) magnetic peak displays a clear disappearance at T^*. We plot the total scattering intensity by summing up the intensities measured at $\mathbf{Q} = (1, 0, 5)$ and (0, 1, 5) in Fig. 3(c). Interestingly, the total scattering intensity in Fig. 3(c) is very similar to the magnetic order parameter measured at $\mathbf{Q} = (1, 0, 1)$ in our previous single-crystal neutron diffraction measurement [15] in Fig. 3(d). This shows that the previous neutron diffraction measured the (1, 0, 1) and (0, 1, 1) peaks simultaneously due to a poor resolution of the neutron measurements. The orthorhombic distortion $\delta = (a - b)/(a + b)$ is displayed in the inset of Fig. 3(c) and shows no significant changes in the orthorhombicity in the studied temperature range, implying the observed temperature dependence is not associated with an additional structural distortion in the ab plane.

The change in intensities of the (1, 0, 5) and (0, 1, 5) magnetic Bragg peaks is a clear indication of Nd magnetic moment reorientation with temperature. The measured intensity ratio I_{105}/I_{015} rapidly deviates from the calculated values for Γ_3 MR indicating that Γ_3 alone cannot explain the unusual temperature dependence. I_{105}/I_{015} does not match with the calculated value for the Γ_2 MR so Γ_2 cannot explain the observation as well. At 1.7 K $< T \leqslant T_{Nd}$, the intensity of

the (0, 1, 5) magnetic peak is rapidly reduced while the peak intensity at $\mathbf{Q} = (1, 0, 5)$ increases. At $T_{\mathrm{Nd}} \leqslant T \leqslant T^*$, a flipping of the ratio I_{105}/I_{015} occurs with the magnetic intensity at $\mathbf{Q} = (1, 0, 5)$ larger than at $\mathbf{Q} = (0, 1, 5)$. Magnetic intensities at $\mathbf{Q} = (h, 0, l)$ can be generated if the Nd moment component becomes available in the a direction as in Γ_6 and Γ_7 MRs in Table I, and these MRs do not produce intensities at $\mathbf{Q} = (0, k, l)$. When the Nd magnetic structure is solely Γ_6 or Γ_7, we would expect a zero intensity at $\mathbf{Q} = (0, k, l)$, which is inconsistent with our observation at $\mathbf{Q} = (0, 1, 5)$. Therefore, we can conclude that the Nd moment configuration at $1.7\ \mathrm{K} < T \leqslant T^*$ consists of Nd moment components both in the a and c directions. In this compound, Fe orders antiferromagnetically with the moments pointing along the a direction [9,10,15]. At $T \leqslant T^*$, the Fe moment is fully developed ($T \ll T_{\mathrm{Fe}} \approx 140$ K) and is coupled to the Nd moment. This coupling between Fe and Nd causes canting of the Nd moment toward the Fe moment direction (the a direction) while the Nd moment prefers to align in the c direction at $T = 1.7$ K.

IV. CONCLUSION

In summary, we have studied the magnetic structure of the NdFeAsO compound using XRMS measurements. We find that the Nd moments are aligned along the c direction, and are arranged antiferromagnetically along the a direction and ferromagnetically along the b and c directions with the Γ_3 magnetic representation at low temperature ($T = 1.7$ K). We find an interesting temperature dependence so that two magnetic reflections behave differently with temperature. Our representation analysis shows that the Nd moments are reoriented toward the a direction in the intermediate temperature range ($1.7 < T \leqslant 15$ K). The unusual temperature dependence and the Nd moment reorientation are due to a strong interaction with the Fe moments. It is interesting to note that among *RE*FeAsO based superconductors (especially with known magnetic structures), Nd and Sm compounds, in which the moments are ordered along the c axis, show higher superconducting transition temperature than the Ce compound which has moments perpendicular to the c axis.

ACKNOWLEDGMENTS

Work at Rutgers University was supported by the U.S. Department of Energy (DOE) under Grant No. DOE: DE-FG02-07ER46382. Work by the Ames group was supported by the Department of Energy, Basic Energy Sciences, Division of Materials Sciences and Engineering, under Contract No. DE-AC02-07CH11358. This research used resources of the Advanced Photon Source, a U.S. Department of Energy (DOE) Office of Science User Facility operated for the DOE Office of Science by Argonne National Laboratory under Contract No. DE-AC02-06CH11357.

[1] Y. Kamihara, T. Watanabe, M. Hirano, and H. Hosono, J. Am. Chem. Soc. **130**, 3296 (2008).
[2] D. C. Johnston, Adv. Phys. **59**, 803 (2010).
[3] M. D. Lumsden and A. D. Christianson, J. Phys.: Condens. Matter **22**, 203203 (2010).
[4] P. Dai, Rev. Mod. Phys. **87**, 855 (2015).
[5] C.-H. Lee, A. Iyo, H. Eisaki, H. Kito, M. Teresa Fernandez-Diaz, T. Ito, K. Kihou, H. Matsuhata, M. Braden, and K. Yamada, J. Phys. Soc. Jpn. **77**, 083704 (2008).
[6] J. Zhao, Q. Huang, C. de la Cruz, S. Li, J. W. Lynn, Y. Chen, M. A. Green, G. F. Chen, G. Li, Z. Li *et al.*, Nat. Mater. **7**, 953 (2008).
[7] S. A. J. Kimber, D. N. Argyriou, F. Yokaichiya, K. Habicht, S. Gerischer, T. Hansen, T. Chatterji, R. Klingeler, C. Hess, G. Behr *et al.*, Phys. Rev. B **78**, 140503(R) (2008).
[8] J. Zhao, Q. Huang, C. de la Cruz, J. W. Lynn, M. D. Lumsden, Z. A. Ren, J. Yang, X. Shen, X. Dong, Z. Zhao *et al.*, Phys. Rev. B **78**, 132504 (2008).
[9] Y. Chen, J. W. Lynn, J. Li, G. Li, G. F. Chen, J. L. Luo, N. L. Wang, P. Dai, C. dela Cruz, and H. A. Mook, Phys. Rev. B **78**, 064515 (2008).
[10] Y. Qiu, W. Bao, Q. Huang, T. Yildirim, J. M. Simmons, M. A. Green, J. W. Lynn, Y. C. Gasparovic, J. Li, T. Wu *et al.*, Phys. Rev. Lett. **101**, 257002 (2008).
[11] A. Marcinkova, E. Suard, A. N. Fitch, S. Margadonna, and J. W. G. Bos, Chem. Mater. **21**, 2967 (2009).
[12] H. Maeter, H. Luetkens, Y. G. Pashkevich, A. Kwadrin, R. Khasanov, A. Amato, A. A. Gusev, K. V. Lamonova, D. A. Chervinskii, R. Klingeler *et al.*, Phys. Rev. B **80**, 094524 (2009).
[13] M. A. McGuire, R. P. Hermann, A. S. Sefat, B. C. Sales, R. Jin, D. Mandrus, F. Grandjean, and G. J. Long, New J. Phys. **11**, 025011 (2009).
[14] D. H. Ryan, J. M. Cadogan, C. Ritter, F. Canepa, A. Palenzona, and M. Putti, Phys. Rev. B **80**, 220503(R) (2009).
[15] W. Tian, W. Ratcliff, M. G. Kim, J.-Q. Yan, P. A. Kienzle, Q. Huang, B. Jensen, K. W. Dennis, R. W. McCallum, T. A. Lograsso *et al.*, Phys. Rev. B **82**, 060514(R) (2010).
[16] S. Nandi, Y. Su, Y. Xiao, S. Price, X. F. Wang, X. H. Chen, J. Herrero-Martín, C. Mazzoli, H. C. Walker, L. Paolasini *et al.*, Phys. Rev. B **84**, 054419 (2011).
[17] A. Marcinkova, T. C. Hansen, and J. W. G. Bos, J. Phys.: Condens. Matter **24**, 256007 (2012).
[18] O. V. Gornostaeva, Low Temp. Phys. **44**, 50 (2018).
[19] J.-Q. Yan, S. Nandi, J. L. Zarestky, W. Tian, A. Kreyssig, B. Jensen, A. Kracher, K. W. Dennis, R. J. McQueeney, A. I. Goldman *et al.*, Appl. Phys. Lett. **95**, 222504 (2009).
[20] J. P. Hill, A. Vigliante, D. Gibbs, J. L. Peng, and R. L. Greene, Phys. Rev. B **52**, 6575 (1995).
[21] D. Watson, E. M. Forgan, W. J. Nuttall, W. G. Stirling, and D. Fort, Phys. Rev. B **53**, 726 (1996).
[22] M. A. Tanatar, A. Kreyssig, S. Nandi, N. Ni, S. L. Bud'ko, P. C. Canfield, A. I. Goldman, and R. Prozorov, Phys. Rev. B **79**, 180508(R) (2009).
[23] M. G. Kim, A. Kreyssig, Y. B. Lee, J. W. Kim, D. K. Pratt, A. Thaler, S. L. Bud'ko, P. C. Canfield, B. N. Harmon, R. J. Mcqueeney, and A. I. Goldman, Phys. Rev. B **82**, 180412(R) (2010).
[24] A. Wills, Physica B: Condens. Matter **276-278**, 680 (2000).
[25] J. P. Hill and D. F. McMorrow, Acta Crystallogr. Sect. A **52**, 236 (1996).